Contributions of vibrational dynamics to the local and excess thermodynamic properties of Cu_3Au surfaces

Weibin Fei, Abdelkader Kara, and Talat S. Rahman
Cardwell Hall, Department of Physics, Kansas State University, Manhattan, Kansas 66502
(Received 3 November 1999)

In a comparative study of the local and excess thermodynamic properties of ordered (100), (110), and (111) surfaces of Cu_3Au using interaction potentials from the embedded atom method, and a real space Green's function method for the calculation of the local vibrational density of states, we find surface effects to be most pronounced on (110). The enhancement of the low frequency modes resulting from the softening of intralayer force constants causes a remarkable lowering of the vibrational free energy on (110). On $Cu_3Au(100)$ the stiffening of interlayer force constants leads to the appearance of modes above the bulk band that reduce the effect of the enhancement of low frequency modes. Atoms on all three surfaces display characteristics that are distinct from those in the bulk.

I. INTRODUCTION

The surfaces of single-crystal bimetallics have been the subject of intense experimental and theoretical investigation in the last two decades because of the interesting possibilities they provide for examining the impact of reduced coordination and symmetry on the nature of the bonding between dissimilar atoms in an alloy. While atomic relaxations, spatial rearrangements (reconstruction), presence of localized vibrational modes, and characteristic local thermodynamics have been the traits of surfaces of monoatomic metals, the presence of two types of entity makes surfaces of bimetallics additionally susceptible to temperature dependent compositional disorder and differential relaxation (rippling). There is also a technological demand for a deeper comprehension of the characteristics of bimetallic surfaces stemming from their importance in heterogeneous catalysis, in high temperature hard materials, in their resistance to corrosion, and in the preparation of ultrathin films. The surfaces of intermetallics like Ni_3Al, Ti_3Al, Pt_3Al, and Cu_3Au have thus been the target of a number of experimental and theoretical investigations.[1,2] In particular, a series of striking experimental observations have made Cu_3Au and its surfaces model systems for theoretical and experimental studies of bimetallics.

In the ordered phase of bulk Cu_3Au, atoms arrange themselves on a face-centered cubic structure such that the Au atoms occupy the corners of an elementary unit cell and the Cu atoms sit at the face-centered sites. At a transition temperature $T_c = 663$ K, which is well below its melting temperature of 1226 K, the bulk system undergoes a first order phase transition[3] in which each site may be occupied randomly by Cu or Au atoms with probabilities of 3/4 and 1/4, respectively, while maintaining the fcc structure. Several experiments and theoretical calculations have found that Cu_3Au surfaces also undergo an order-disorder transition; however, unlike the bulk transition, this is second order[4–7] with the disorder initiating at temperatures well below the bulk transition temperature. The driving force for this surface transition is not well understood, particularly because the system retains its short range order, as revealed in the segregation profiles of the surface compositions in which the Au concentration may be enhanced or remain unchanged during the phase transition.[8]

The issue of the mechanisms underlying the order-disorder transition in bulk Cu_3Au and other bimetallics also remains, as yet, unresolved. Experimental and theoretical investigations aimed at understanding the processes that drive the transition have rightly examined the contributions to the free energy differences between the ordered and disordered states. Although the contribution of the vibrational entropy to the free energy difference has long been considered to be important, earlier calculations focused mainly on the role of the configurational entropy difference in causing this transition. The subject has received renewed attention since recent experimental data on several bimetallics[9–11] indicate that the vibrational entropy may indeed play a significant role in the bulk order-disorder transition. Related calculations using many-body interaction potentials have disagreed as to whether this vibrational entropy contribution results from the change in volume due to disordering[12] or from the presence of grain boundaries.[13] Using results from first principles calculations, Ozoliņš *et al.*[14] have calculated the effect of vibrational free energy on the order-disorder transition temperature in bulk Cu-Au alloys. With regard to surfaces, the situation is even more complicated as a result of lower symmetry and the more complex nature of the bonding. Vibrational free energy may in fact play an even stronger role in surface structural phase transitions because of the presence of localized vibrational modes whose characteristics depend on the local atomic environment. In this regard, the surfaces of Cu_3Au provide an interesting variety of regions of low coordinations. The stacking of planes for $Cu_3Au(111)$, for example, have the repeat pattern *ABC* of fcc (111) planes with each plane containing 75% Cu and 25% Au and the in-plane coordination of the surface atoms is 6 (see Fig. 1). On the other hand, $Cu_3Au(100)$ and $Cu_3Au(110)$ consist of *AB* stacking planes alternately containing 50% Cu and 50% Au, and 100% Cu. The surface termination in case of a (100) or (110) surface may thus be either mixed (1:1), or the so-

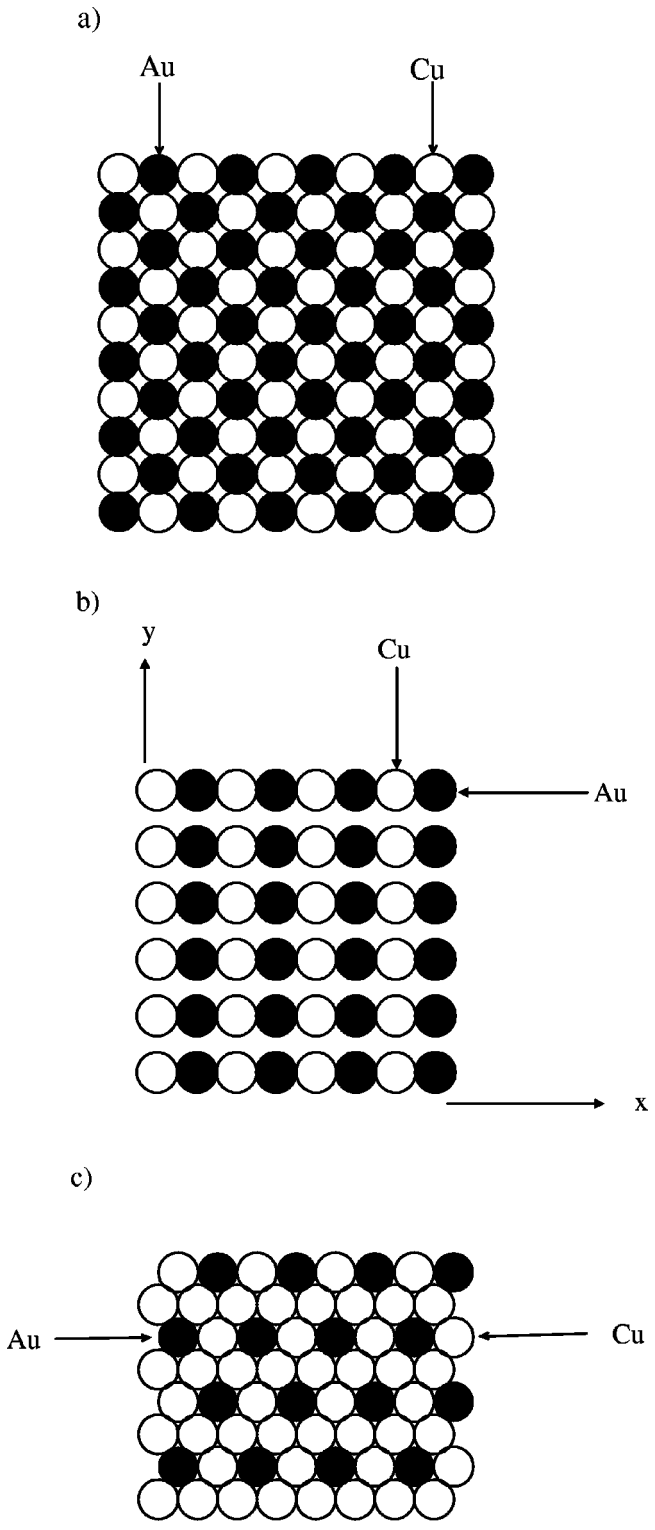

FIG. 1. Structural arrangement in the top layer of ordered (a) $Cu_3Au(100)$, (b) $Cu_3Au(110)$, and (c) $Cu_3Au(111)$.

called ''Au poor''(1:0). For the mixed termination, the in-plane coordination of the surface atoms on (100) and (110) is 4 and 2, respectively.

The (100) surface of the ordered phase has been shown from a number of experiments to possess bulk termination plane *A* with 50% Cu and 50% Au ordered in a $c(2\times2)$ arrangement.[15–17] Theoretical calculations also support this mixed composition and predict a small amount of surface rippling. Early Monte Carlo calculations[18] using interaction potentials from the embedded atom method[19] (EAM) predict a rippling of 0.18 Å, in agreement with results reported by Wallace and Ackland[20] using a different many-body interaction potential. Using yet another type of semiempirical potential suitable particularly for alloys, Kobistek *et al.*[21] found a rippling of 0.15 Å for the (100) surface. Recent low energy ion scattering experiments have confirmed that indeed Au atoms in the surface layer are about 0.12 Å above the Cu atoms in the same layer.[22]

The (110) and (111) surfaces of Cu_3Au have not been studied as extensively as the (100). For $Cu_3Au(110)$, while the surface layer has been recognized to be of mixed composition, the exact structure is still not clear.[23] Theoretical calculations suggest a buckling of the surface and an additional in-plane contraction.[20,21] For $Cu_3Au(111)$, reflection high energy electron diffraction experiments confirm that every layer has bulk stoichiometry, i.e., 25% Au and 75% Cu.[24] In addition, theoretical calculations predict a surface rippling of 0.17 Å.[21]

Motivated by the above findings, we present here a systematic, comparative study of the vibrational dynamics and thermodynamics of the low Miller index, ordered surfaces of Cu_3Au, as a first step in developing a framework by which we can evaluate the contribution of vibrational entropy to the temperature dependent surface order. We examine first the structural properties of Cu_3Au (100), (110), and (111) surfaces and establish the validity of our model calculations by comparing results with previous work. We then calculate the local vibrational density of states of the ordered phases of these three surfaces of Cu_3Au and use them to examine the local and surface excess thermodynamic properties. The rest of the paper is organized as follows. In Sec. II we present the model system and some details of the calculations. In Sec. III, we present the results with discussion. Finally, in Sec. IV we summarize our conclusions.

II. THEORETICAL DETAILS

For calculations of the structural and dynamical properties we construct Cu_3Au surface systems consisting of about 1000 to 2500 atoms distributed over 17 or 18 layers. For the (100) and (110) surfaces we use 17 layers, while for the (111) surface 18 layers are needed to obtain equivalent surfaces on the two sides. The number of atoms in each layer ranges from 100 for $Cu_3Au(100)$, 64 for $Cu_3Au(110)$, and 144 for $Cu_3Au(111)$ surfaces. These model system sizes were chosen after a series of tests established that the results of the calculations were devoid of finite size effects. In this work we have assumed that the top layer of $Cu_3Au(100)$ and $Cu_3Au(110)$ has a mixed composition of 50% Cu and 50% Au, while the (111) surface has the bulk stoichiometry, following the general consensus from previous experimental and theoretical studies.[15] Figure 1 shows a top view of the three surfaces.

We use EAM potentials to describe the interaction between the atoms in the model systems. As is well known, this method provides empirical many-body interaction potentials for the fcc metals Ag, Au, Cu, Ni, Pd, Pt, and their alloys that successfully depict a variety of bulk and surface properties of these systems. Our calculations of the bulk properties

of Cu_3Au using the EAM potentials give relatively reliable results. However, as we shall see, there is a problem with regard to the calculated surface energies for the two possible terminations of $Cu_3Au(100)$ and $Cu_3Au(110)$. The details of the EAM and its applications to surface and bulk systems can be found in the review article by Daw *et al.*[19]

In the calculation, the surface systems are first constructed in their bulk terminated positions and then relaxed, using a conjugated gradient scheme, to yield the equilibrium configuration at 0 K. The force constant matrix is next calculated from analytical expressions for the partial second derivatives of the EAM potentials.[19] We then use a real space Green's function method, as developed by Wu and co-workers,[25] to obtain the local vibrational density of states. The basic calculation involved in this technique is the solution of the eigenvalue problem

$$H\psi = z\psi, \tag{1}$$

where H is the Hamiltonian, which in our case is the force constant matrix. Equivalently, one can use the Green's function operator:

$$G = (zI - H)^{-1}, \tag{2}$$

the trace of which is related to the normalized vibrational density of states as represented by the function

$$g(\omega^2) = -\frac{1}{3n\pi}\lim_{\epsilon\to 0}\mathrm{Im}\,\mathrm{Tr}[G(\omega^2 + i\epsilon)]. \tag{3}$$

The frequency dependent vibrational density of states $N(\omega)$ follows directly from

$$N(\omega) = 2\omega g(\omega^2). \tag{4}$$

This real-space method has the advantage that it makes no use of the concepts of wave vectors and Brillouin zones. Since it does not require the systems to be periodic, it is very appropriate for studying complex systems with low symmetry. The only prerequisite to this method is that the interatomic potential between the atoms in the system be of finite range, so that the force constant matrix can be written in a block tridiagonal form. For the system of interest here, the force constant matrix is constructed in a layer-by-layer form in which the locality for (100) and (110) surfaces consists of two layers (corresponding to AB stacking), while that for the (111) surface consists of three layers (ABC stacking).

Once the local vibrational density of states is calculated, we can easily determine the thermodynamic functions of the system which, in the harmonic approximation, are given by

$$F_{vib} = k_B T \int_0^\infty \ln\left[2\sinh\left(\frac{\hbar\omega}{2k_BT}\right)\right] N(\omega)\,d\omega, \tag{5}$$

$$S_{vib} = k_B \int_0^\infty \left[\frac{\hbar\omega}{2k_BT}\coth\left(\frac{\hbar\omega}{2k_BT}\right) - \ln\left(2\sinh\frac{\hbar\omega}{2k_BT}\right)\right] N(\omega)\,d\omega, \tag{6}$$

TABLE I. Unrelaxed and relaxed Cu_3Au surface energies (in erg/cm^2).

Surface	Unrelaxed	Relaxed
(100) 1:1	1309	1260
(100) 1:0	997	970
(110) 1:1	1441	1395
(110) 1:0	1124	1043
(111) 3:1	1022	993

$$C_v = k_B T \int_0^\infty \left(\frac{\hbar\omega}{2k_BT}\right)^2 \frac{1}{\sinh^2(\hbar\omega/2k_BT)} N(\omega)\,d\omega, \tag{7}$$

$$\langle u_{i\alpha}^2\rangle = \frac{\hbar}{2M_i}\int_0^\infty \frac{1}{\omega}\coth\left(\frac{\hbar\omega}{2k_BT}\right) N_{i\alpha}(\omega)\,d\omega, \tag{8}$$

where F_{vib}, S_{vib}, C_{vib}, and $\langle u_\alpha^2\rangle$ are, respectively, the vibrational free energy, the vibrational entropy, the lattice heat capacity, and the mean square atomic displacements along the Cartesian direction α, and $N(\omega)$ is the calculated total vibrational density of states. $N_{i\alpha}(\omega)$ is the local vibrational density of states of atom i, with mass M_i, along the direction α.

III. RESULTS AND DISCUSSION

In Table I we present our calculated surface energies for the three surfaces. For both $Cu_3Au(100)$ and $Cu_3Au(110)$ we find the pure Cu terminated surface (1:0) to have lower energy than the mixed terminated one (1:1). The EAM potentials thus favor a surface termination which is inconsistent with the results of previous experimental and theoretical studies.[15,21] This inconsistency may be traced to the inadequacy of the EAM potentials in predicting surface energies.[19] As we shall see, despite this limitation, EAM potentials give reasonable results for the structural properties of the mixed terminated surfaces of $Cu_3Au(100)$ and $Cu_3Au(110)$.

A. Surface relaxation and force constants

Our calculated surface relaxations at 0 K, as a percentage of the bulk interlayer spacing, for the mixed terminated (100) and (110) surfaces as well as the stoichiometric (111) termination are presented in Table II. Note that the interlayer spacings for (100), (110), and (111) planes of bulk Cu_3Au are 1.8738 Å, 1.3250 Å, and 2.165 Å, respectively. These results are in qualitative agreement with the calculations by Kobistek *et al.*,[21] which gave the first layer contraction of Cu

TABLE II. Relaxations of low Miller index Cu_3Au surfaces (in percentage of bulk interlayer distance).

Atom type	(100)	(110)	(111)
Cu_1	−7.90	−8.45	−2.67
Au_1	−0.52	−5.30	4.45
Cu_2	1.20	0.76	1.80
Au_2			0.38

TABLE III. Force constant matrices $K_{\alpha\beta}$ [in eV Å^{-1} (unit mass)$^{-1}$] for the interaction between the nearest neighbor atoms on $Cu_3Au(100)$ and in the bulk. In all tables subscripts label the layer of the atom considered.

Atoms		Surface			Bulk		
Au_1-Cu_1	x	0.0947	0.0000	0.0000	0.3389	0.0000	0.0000
	y	0.0000	−3.2942	−1.1794	0.0000	−4.5356	0.0000
	z	0.0000	0.2253	0.0125	0.0000	0.0000	0.3515
Cu_1-Cu_2	x	−1.6790	2.4463	−3.1334	−0.8965	1.2833	−1.7707
	y	2.4463	−1.6789	3.1334	1.2833	−0.8965	1.7707
	z	−3.1734	3.1733	−3.7416	−1.5757	1.5757	−2.1898
Au_1-Cu_2	x	−0.8431	−1.1131	−1.5436	−0.8618	−1.2082	−1.7035
	y	−1.1131	−0.8431	−1.5436	−1.2082	−0.8618	−1.7035
	z	−1.9912	−1.9912	−2.6297	−1.7032	−1.7032	−2.0810

atoms on the (100) surface as −9.10%, and the corresponding values for (110) and (111) surfaces as −9.21% and −4.47%, respectively. The differential relaxation of the Au and the Cu atoms in the first layer gives rise to the expected phenomenon of rippling on a binary alloy surface. Our results in Table II, which predict a rippling of 0.14 Å for Au atoms, are in close agreement with experimental data[22] and other theoretical results.[20,21] The calculated rippling values of 0.04 Å for $Cu_3Au(110)$ and 0.15 Å for $Cu_3Au(111)$ from Table II are also comparable to those found in previous calculations.[21]

From the comparison between our calculated surface relaxations, related experimental data, and other theoretical results, we conclude that the EAM potentials provide a reliable representation of the characteristics of the mixed terminated (100) and (110) surfaces, as well as the stoichiometric structure for the (111) surface of Cu_3Au. For the relaxed configuration of mixed terminated surfaces, we proceed next with the analysis of our calculated force constant matrix elements $K_{\alpha\beta}$ between the nearest neighbor surface atoms, where α and β stand for Cartesian components, as presented in Tables III–V. For each case, the values of the force constants between corresponding bulk atoms are also included. In the tables and in the rest of the paper we label the atoms in layer i as M_i, where M stands for Au or Cu. From Table III we find that the force constant K_{yy}, or by symmetry K_{xx} [since the Au_1 atom has nearest neighbor Cu_1 atoms along the x and y axes), between the Au and Cu atoms in the top layer on $Cu_3Au(100)$] is reduced by 27% from the bulk value. Meanwhile, the force constants K_{zz}, for the interactions Cu_1-Cu_2 and Au_1-Cu_2 along the direction perpendicular to the (100) surface, have stiffened by 70.9% and 26.4%, respectively. There are several other noticeable differences in the related surface and bulk force constants. Similarly, for the (110) surface, in Table IV, the force constant K_{xx}, representing the interaction Cu_1-Au_1, has softened by 40.6% compared to the bulk. Since on this surface the coupling in the z direction is actually the strongest among nearest neighbors in planes i and $(i-2)$, we compare K_{zz} for Cu_1-Au_3 and Au_1-Cu_3 with their bulk counterparts. From Table IV, we find 51% and 45% stiffening for Cu_1-Au_3 and Au_1-Cu_3, respectively. Note that the stiffening is slightly larger for Cu_1-Au_3 owing to a small rippling. For the (111) surface, Cu atoms in the first layer also have nearest neighbor Cu atoms, in addition to Au atoms in the layer. In addition, there are Au atoms in the second layer which are nearest neighbors of both Cu and Au atoms in the surface layer. Thus five sets of surface force constants need to be examined and compared to the values in the bulk. Table V show that the force constant K_{xx} for the intralayer Cu_1-Cu_1 interaction has softened by 36.5% and that for Cu_1-Au_1 by 22.8%. In contrast, the force constant K_{zz} has stiffened by 55.9%, 14.6%, and 15.6% for the Cu_1-Cu_2, Au_1-Cu_2, and Cu_1-Au_2, interactions, respectively. In summary, for all surfaces there is a softening of the intraplanar force field that scales inversely with the coordination: 22.8%, 27.0%, and 40.6% for Au_1-Cu_1 interactions on (111), (100), and (110) surfaces, respectively (with coordination 9,

TABLE IV. Force-constant matrices $K_{\alpha\beta}$ [in eV Å^{-1} (unit mass)$^{-1}$] for the interaction between the nearest neighbor atoms on Cu_3Au (110) and in the bulk.

Atoms		Surface			Bulk		
Cu_1-Au_1	x	−2.6599	0.0000	−0.2339	−4.4652	0.0000	−0.0005
	y	0.0000	−0.0411	0.0000	0.0000	0.3349	0.0000
	z	1.4628	0.0000	−0.1490	−0.0005	0.0000	0.3223
Cu_1-Au_3	x	0.3038	0.0000	0.0000	0.3270	0.0000	0.0000
	y	0.0000	0.3198	0.0000	0.0000	0.3398	0.0000
	z	0.0000	0.0000	−6.4482	0.0000	0.0000	−4.4205
Au_1-Cu_3	x	0.5184	0.0000	0.0000	0.3340	0.0000	0.0000
	y	0.0000	0.5130	0.0000	0.0000	0.3468	0.0000
	z	0.0000	0.0000	−6.7661	0.0000	0.0000	−4.4844

TABLE V. Force constant matrices $K_{\alpha\beta}$ [in eV Å^{-1} (unit mass)$^{-1}$] for the interaction between the nearest neighbor atoms on Cu_3Au (111) and in the bulk.

Atoms		Surface			Bulk		
Cu_1-Cu_1	x	−2.9324	−0.1050	−0.5824	−4.6170	−0.0805	−0.1120
	y	0.1050	0.2238	−0.1058	0.0805	0.3248	−0.0965
	z	0.5824	−0.1058	0.0109	0.1120	−0.0965	0.2536
Cu_1-Au_1	x	−3.5020	−0.0155	−0.2359	−4.5391	−0.0004	−0.0016
	y	−0.0533	0.1852	−0.0067	−0.0004	0.3484	−0.0059
	z	0.9979	0.0055	0.0556	−0.0017	−0.0059	0.343
Cu_1-Cu_2	x	−1.4149	1.0405	−3.1599	−0.8942	0.7002	−2.0678
	y	0.8849	−0.1662	1.5999	0.5412	−0.1775	1.0639
	z	−3.1959	1.8588	−4.5244	−1.9552	1.2591	−2.9042
Au_1-Cu_2	x	−0.7773	−0.5821	1.7578	−0.8627	−0.6911	1.9728
	y	−0.5821	−0.1051	1.0149	−0.6911	−0.0647	1.1390
	z	2.1068	1.2164	−3.2990	1.9726	1.1389	−2.8788
Cu_1-Au_2	x	−0.9937	−0.8025	2.2205	−0.8639	−0.6922	1.9757
	y	−0.8025	−0.0671	1.2820	−0.6922	−0.0646	1.1406
	z	2.3646	1.3652	−3.3225	1.9758	1.1407	−2.8826

8, and 7). On the other hand, there is a stiffening of the force field perpendicular to the surface with the effect being larger for those involving Cu_1 than Au_1, as a consequence of the nature of the surface rippling.

B. Vibrational density of states

In Figs. 2–4, we present the local density of states (LDOS) for atoms down to the fourth layer on $Cu_3Au(100)$, $Cu_3Au(110)$, and $Cu_3Au(111)$, together with the density of states for the atoms in bulk Cu_3Au. Note that the maximum phonon frequency in the bulk is smaller than that of bulk Cu ($\simeq$8 THz), partly because of the larger lattice constant of Cu_3Au (3.75 Å vs 3.61 Å) and partly because of the presence of Au atoms. Atoms in the first layer for all three surfaces have significantly different local density of states as compared to that in the bulk. On each surface there is an enhancement of modes in the lower frequency range [up to 4 THz on (100), 2 THz on (110), and 3 THz on (111)]. The local densities of states of the second layer atoms on the (100) and (110) surfaces also show some variations from the bulk value: on (100) there is the presence of modes above the bulk phonon frequencies, while on (110) there is continued enhancement of the low frequency modes. Since the local densities of states of the third and the fourth layer atoms are similar to those of the atoms in the bulk for all three surfaces, it is reasonable to focus our discussion only on the first and second layer atoms, in this comparative study of the dynamics of the three surfaces.

To gain further insights we have plotted the x, y, and z resolved local densities of states for the Cu and Au atoms in the top layer of the the (100), (110), and (111) surfaces, in Fig. 5. These figures show that for all three surfaces all components of the LDOS of Au and Cu atoms in the first layer have some enhancement in the low frequency range. Note, however, the differences in the LDOS's in the 0–2 THz

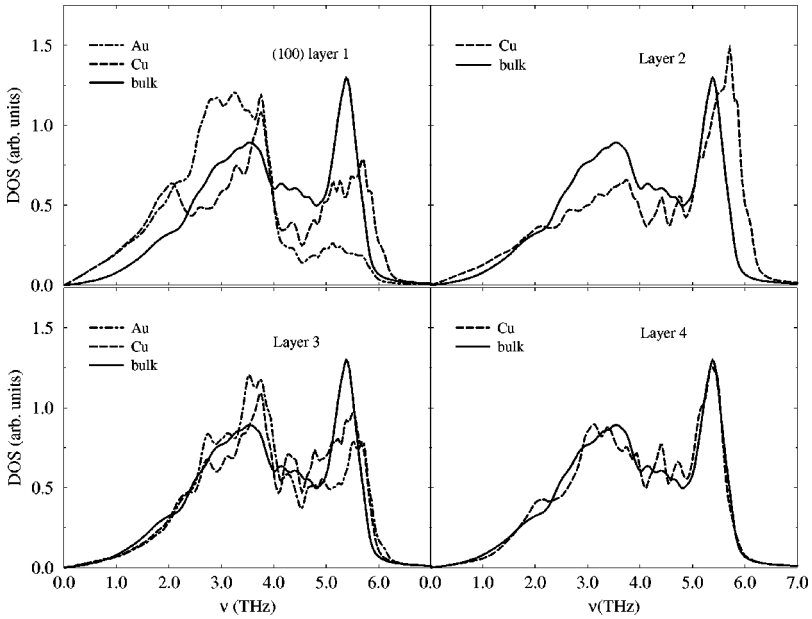

FIG. 2. Local vibrational densities of states for Cu and Au atoms in top four layers of $Cu_3Au(100)$.

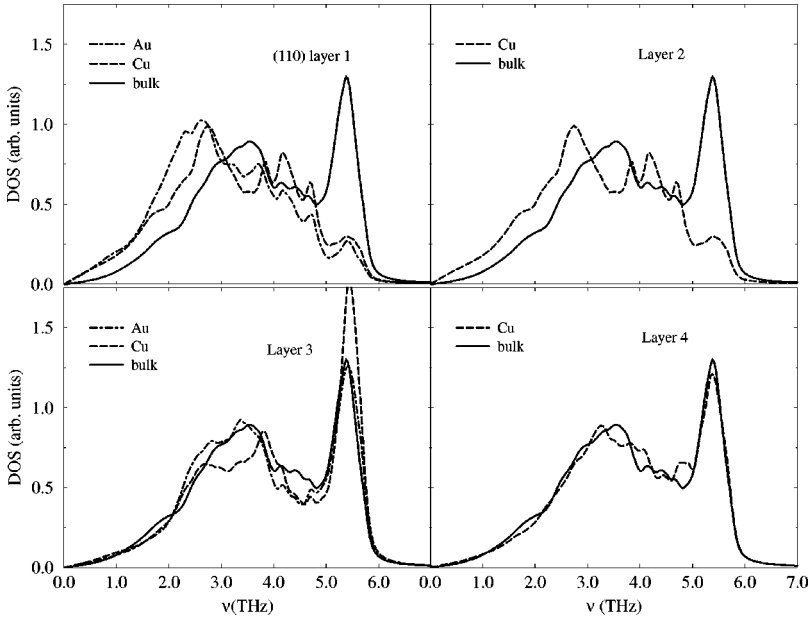

FIG. 3. Local vibrational densities of states for Cu and Au atoms in top four layers of $Cu_3Au(110)$.

range for the three surfaces, particularly the contribution of the modes with atomic displacements along the surface normal.

The comparison of the LDOS's for the Au atoms on the three surfaces is also very interesting. Despite the compositional similarity between the (100) and (110) surfaces, the LDOS's of the Au atoms on the (100) and (111) surfaces have similar features (concentration in the 2–4 THz range, depletion in the higher frequency range), while on the (110) surface Au atoms have their LDOS's distributed over a larger frequency range. It is remarkable that the LDOS of $Cu_3Au(110)$ exhibits distribution above 5 THz, the maximum bulk phonon frequency for pure Au. These higher frequency modes in Fig. 5(e) indicate the extent of the coupling between the Au and Cu atoms on these surfaces. On turning to the LDOS's for the Cu atoms in Fig. 5, we find the characteristics on $Cu_3Au(100)$ to be quite distinct as the modes spread over the entire frequency range, extending well beyond the maximum bulk phonon modes. Here the (110) surface again distinguishes itself with the striking similarity between the LDOS's of the Au and the Cu atoms. As we shall see, these comparative features in the LDOS's control the differences in the local thermodynamics on the three surfaces. Although we have not calculated the dispersion of specific surface phonon modes, the LDOS's in Figs. 5(a) and 5(d) exhibit features that may be compared with experimental data. In the He-atom surface scattering experiments by Gans *et al.*[26] modes were found at 3.12 THz and 1.80 THz at the zone boundaries of $Cu_3Au(100)$, which they ascribed to the vertical motion of the Au and Cu surface atoms, respectively. In our calculations we find peaks in the LDOS's of Cu and Au in Figs. 5(a) and 5(d) corresponding to these frequencies.

To get some qualitative ideas about the red- or blueshifts of the LDOS's, we present in Table VI the weighted frequencies (one-half the number of modes lie above it and the other

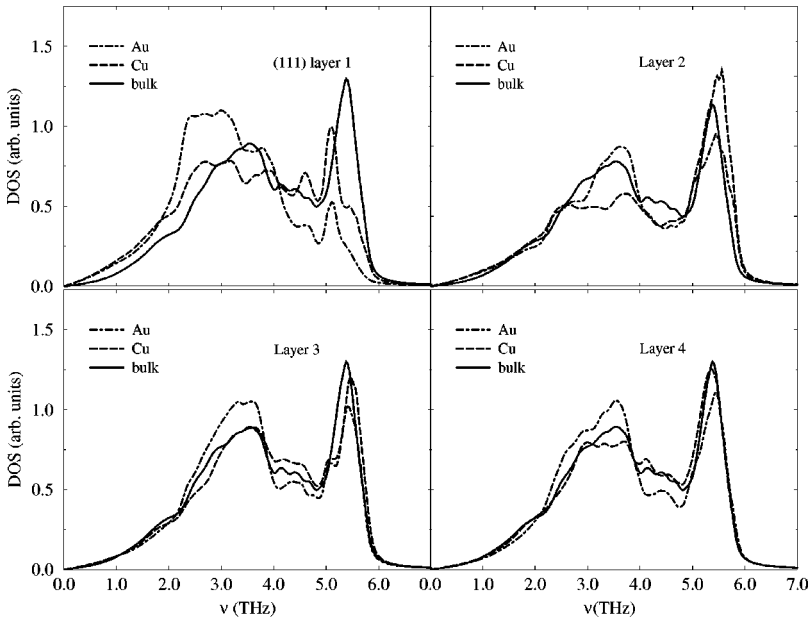

FIG. 4. Local vibrational densities of states for Cu and Au atoms in top four layers of $Cu_3Au(111)$.

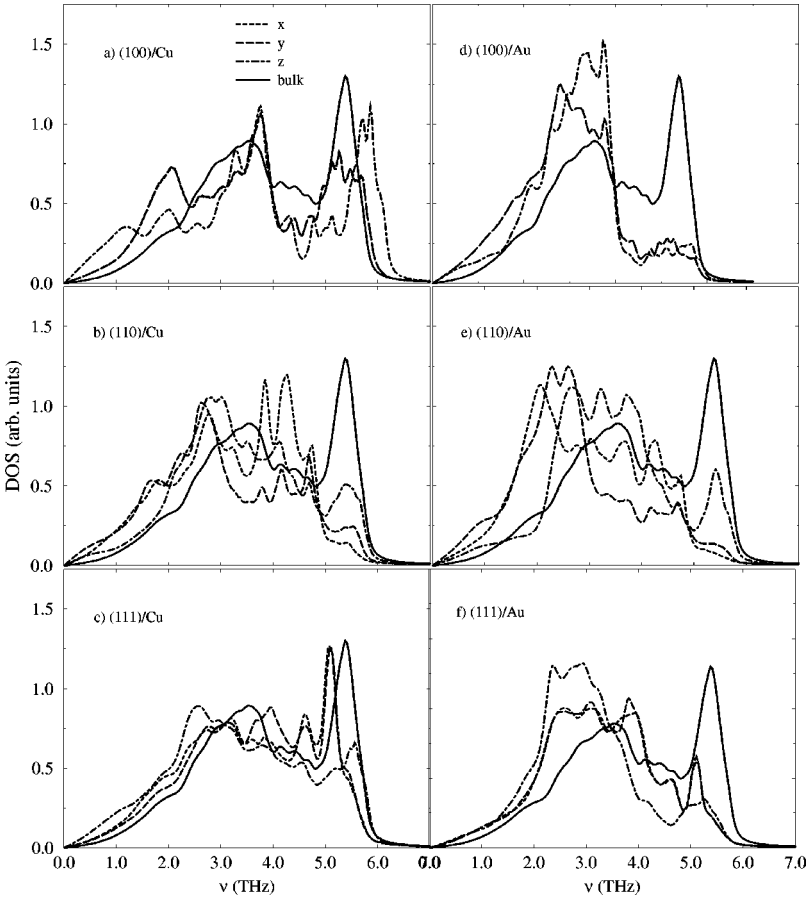

FIG. 5. The *x*, *y*, and *z* resolved local vibrational densities of states for the Cu (a)–(c) and Au (d)–(f) atoms in first layer of the (100), (110), and (111) surfaces of Cu_3Au.

below) of the LDOS's. In each case we find the weights to be shifted to frequencies lower than that of the bulk. This phenomenon is related to the softening of the intraplanar force constants in the top layer, on all three surfaces, as described earlier. The table shows the Au atoms to be more redshifted than their Cu counterparts. Also, for both Au and Cu atoms the shift to lower frequencies is most prominent on the (110) surface. This is not only because (110) has the largest percentage of force constant softening in the direction of interest, but also because of the smaller in-plane coordination number [2, compared to 4 and 6 for (100) and (111), respectively]. In the case of the densities of states of modes with atomic displacements perpendicular to the surface, the overall shifts in weight result from a combination of stiffening of force constants and loss of nearest neigbors above the surface. The tendency of the latter to soften the mode frequency thus competes with that of the former to push it to higher frequencies.

TABLE VI. The weighted frequency in THz of the LDOS's. Note that the corresponding value for the bulk LDOS is 3.79 THz.

Atom	Component	Cu_3Au surfaces		
		(100)	(110)	(111)
Au	*x*	2.98	2.86	3.22
	y	2.98	2.53	3.22
	z	3.19	3.34	2.89
Cu	*x*	3.55	3.28	3.58
	y	3.55	2.86	3.70
	z	3.64	3.28	3.28

C. Surface thermodynamic functions

With the calculated local vibrational density of states in Figs. 2 –5 we are in a position to determine both the local contribution from each type of atom in a layer, and the total excess contribution from the surface, to the thermodynamic properties of Cu_3Au. The former is a useful measure of how the local vibrational density of states of each type of surface atom impacts the overall temperature dependent characteristics of the surface. Local quantities like the mean square vibrational amplitudes of individual surface atoms, or the average values of those in a layer, provide indications of the propensity of a surface to disorder or premelt. They are also important for proper analysis of structural experimental data. Comparative examination of the atomic or layer-by-layer contributions to the vibrational entropy is necessary meanwhile for consideration of relative surface stability. These local contributions to the vibrational thermodynamic functions are obtained by using the corresponding local vibrational densities of states in Eqs. (5)–(8). The surface excess thermodynamic functions, on the other hand, provide an overall measure of the amount by which a particular thermodynamic function for a surface system differs from that of the bulk. It is the excess over the value in the bulk. The excess quantities are calculated by using in Eqs. (5)–(8) the difference in the LDOS for locality *l* from the bulk LDOS and summing over all *l*. Hence, for a vibrational thermodynamic quantity *X*, the excess, local, and bulk values are related by

$$X_{vib}^{excess}=\sum_{l}\,(X_{vib}^{l}-X_{vib}^{bulk}). \tag{9}$$

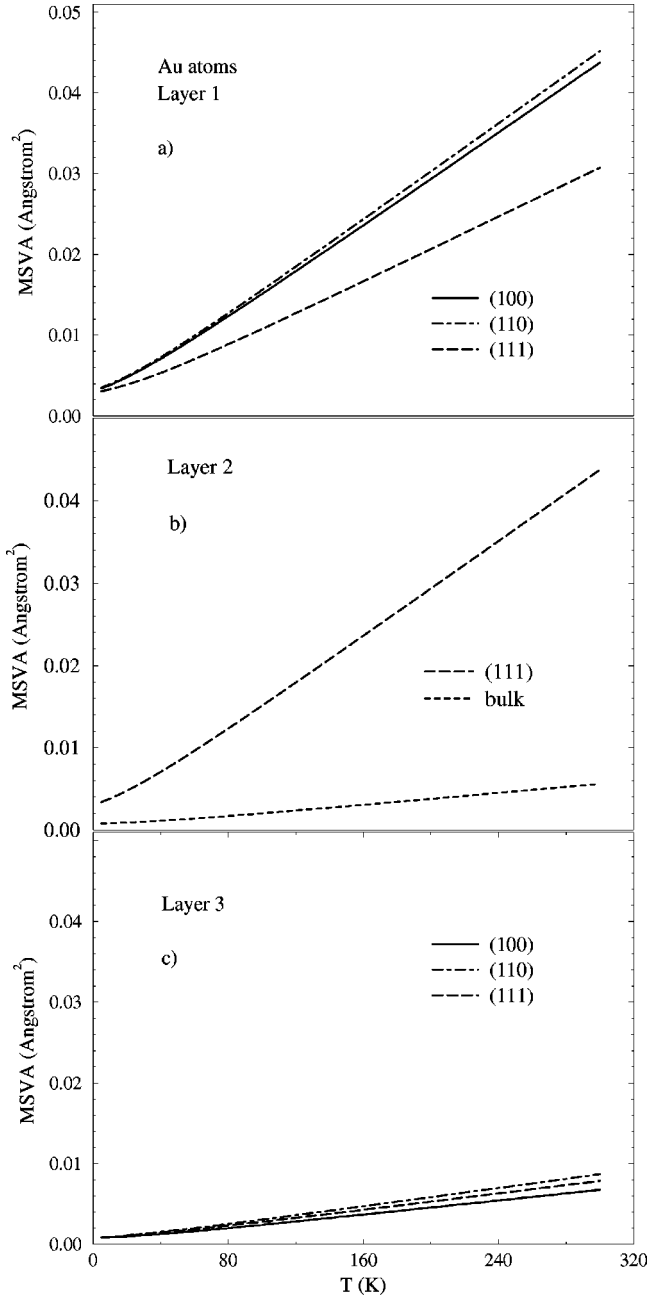

FIG. 6. Calculated mean square vibrational amplitudes for Au atoms in the top three layers of the (100), (110), and (111) surfaces of Cu_3Au.

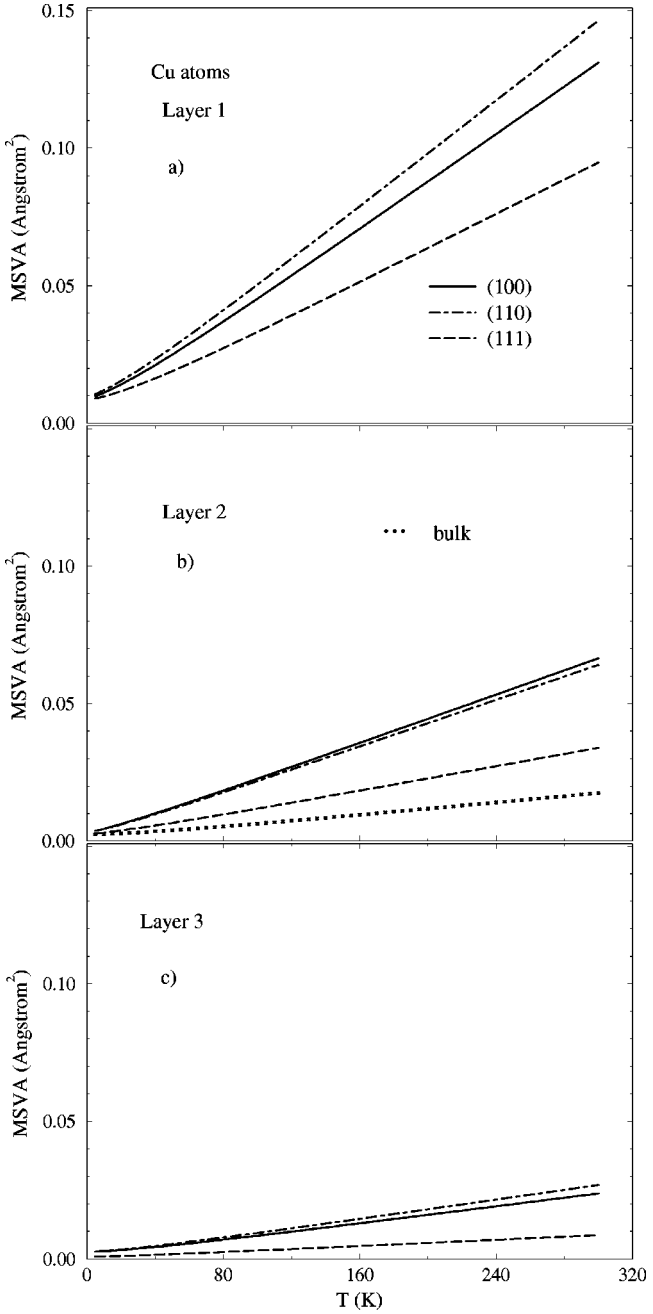

FIG. 7. Calculated mean square vibrational amplitudes for Cu atoms in the top three layers of the (100), (110), and (111) surfaces of Cu_3Au.

In the subsections below we first examine the mean square vibrational amplitudes of the constituent atoms in the first two layers of $Cu_3Au(100)$, (110), and (111). This is followed by a comparative study of the local vibrational entropies and the free energies of the same sets of local regions. At the end of the section, we present our results for the surface excess thermodynamic functions.

1. Mean square vibrational amplitudes

A comparison in Fig. 6 of the mean square vibrational amplitudes (MSVA's) of the Au atoms in the top layers of Cu_3Au (100), (110), and (111) shows those for (100) and (110) surfaces to be almost equal, and larger than that of the Au atoms on the (111) surface, reflecting the similarity in the composition of the (100) and (110) surfaces. Only $Cu_3Au(111)$ has Au atoms in the second layer, and it is interesting that its MSVA is larger than that of the Au atoms in its first layer. For all three surfaces, the MSVA in the third layer shows only small differences from that of the atoms in the bulk.

A similar comparison in Fig. 7 for Cu atoms shows that the amplitudes for the first layer are largest on (110), followed by those on (100) and (111). Note that for all three surfaces the mean square vibrational amplitude of the Cu atoms is about three times larger than that of Au. This may be ascribed to the difference in mass between Au and Cu atoms. The linear dependence of the MSVA in these figures is a consequence of the harmonic approximation, which we

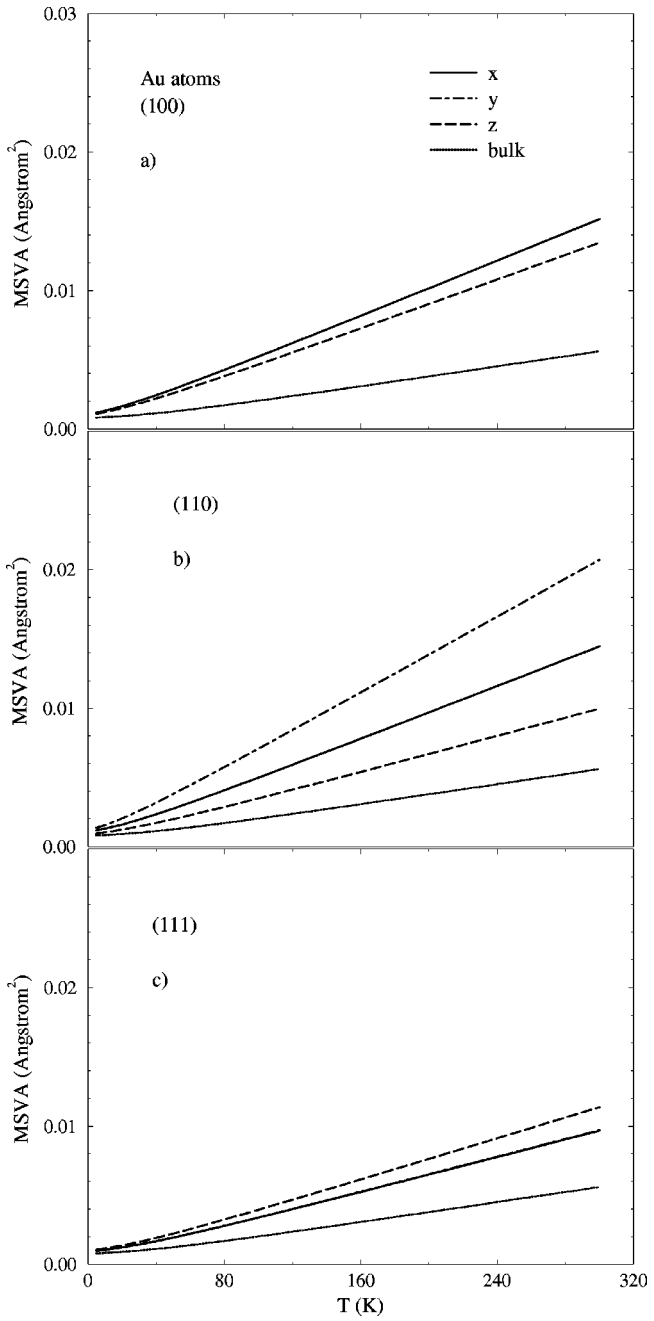

FIG. 8. The *x*, *y*, and *z* components of the mean square vibrational amplitudes of the top layer Au atoms on the three surfaces.

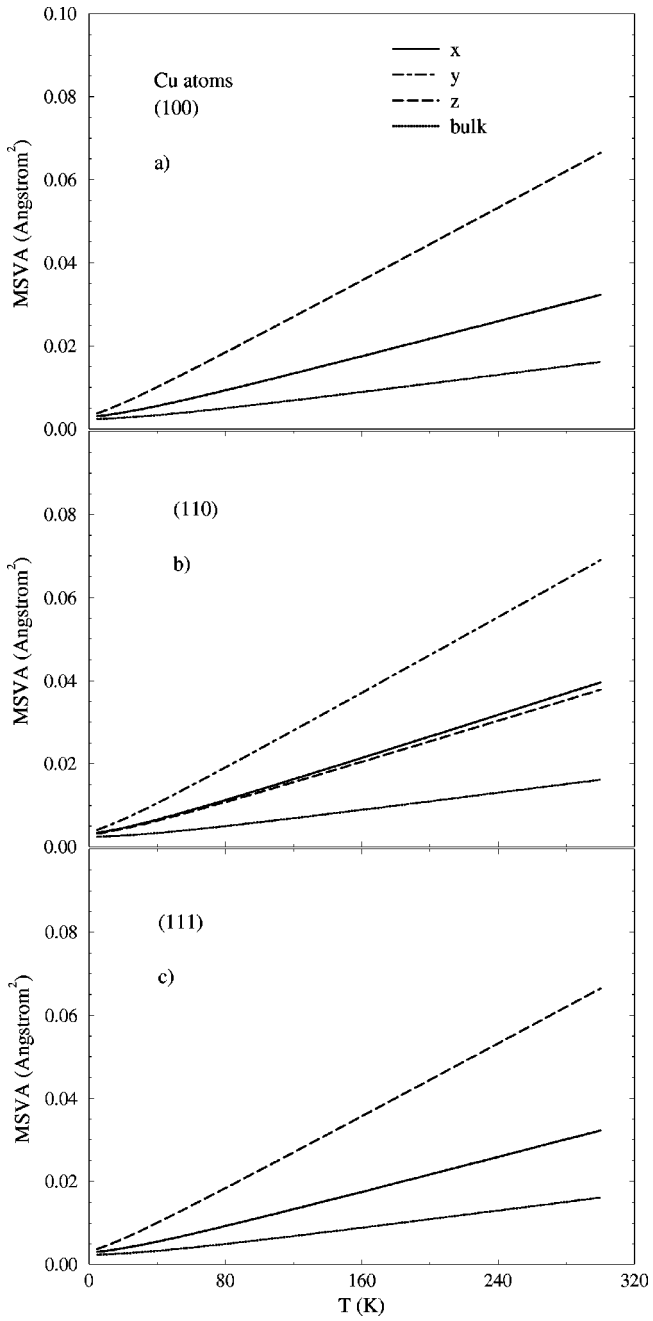

FIG. 9. The *x*, *y*, and *z* components of the mean square vibrational amplitudes of the top layer Cu atoms on the three surfaces.

expect to be valid for the temperature range in Figs. 6–12. The three components of the MSVA for the Au atoms in the top layers in Fig. 8 show the most pronounced anisotropy to be on the (110) surface, for which the *y* component is the largest. This is not surprising because of the pronounced softening of the force constants in this direction and larger space between atoms. Similar plots of the *x*, *y*, and *z* components of the MSVA of the Cu atoms in the top layers of the three surfaces, in Fig. 9, show pronounced anisotropy between the in-plane and out-of-plane directions on all three surfaces.

2. Local contributions to vibrational entropy

The contributions of the Au and Cu atoms in the top two layers of the three surfaces to the vibrational entropy in the temperature range 0–300 K are summarized in Fig. 10. On all three surfaces and for the entire temperature range the contribution is largest for the Au atoms in the top layer, followed by that of Cu atoms in the same layer. It is interesting that at 300 K (for example) Au atoms contribute about 0.47 meV/K to the entropy of the (100) and (110) surfaces, and about 0.45 meV/K to the (111) surface. On $Cu_3Au(110)$, Cu atoms in the top layer make a contribution only slightly less than that of the Au atoms ($\simeq$0.455 meV/K), while on $Cu_3Au(100)$ and $Cu_3Au(111)$ the Cu atoms contribute $\simeq$0.43 meV/K. The second layer atoms on all three surfaces add about 0.4 meV/K to the vibrational entropy. The similarities and differences in these curves in the relative contributions of the Au and Cu atoms on the three surfaces are all

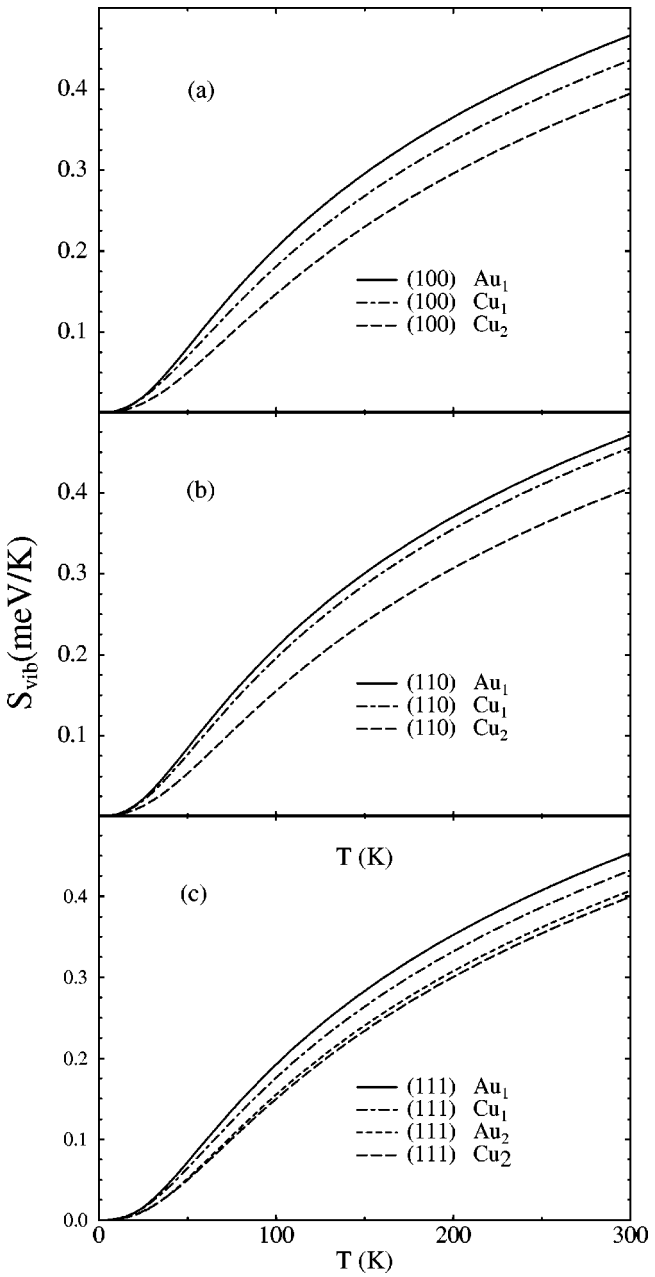

FIG. 10. Local vibrational entropy of Au and Cu atoms in the top two layers of Cu_3Au (a) (100), (b) (110), and (c) (111).

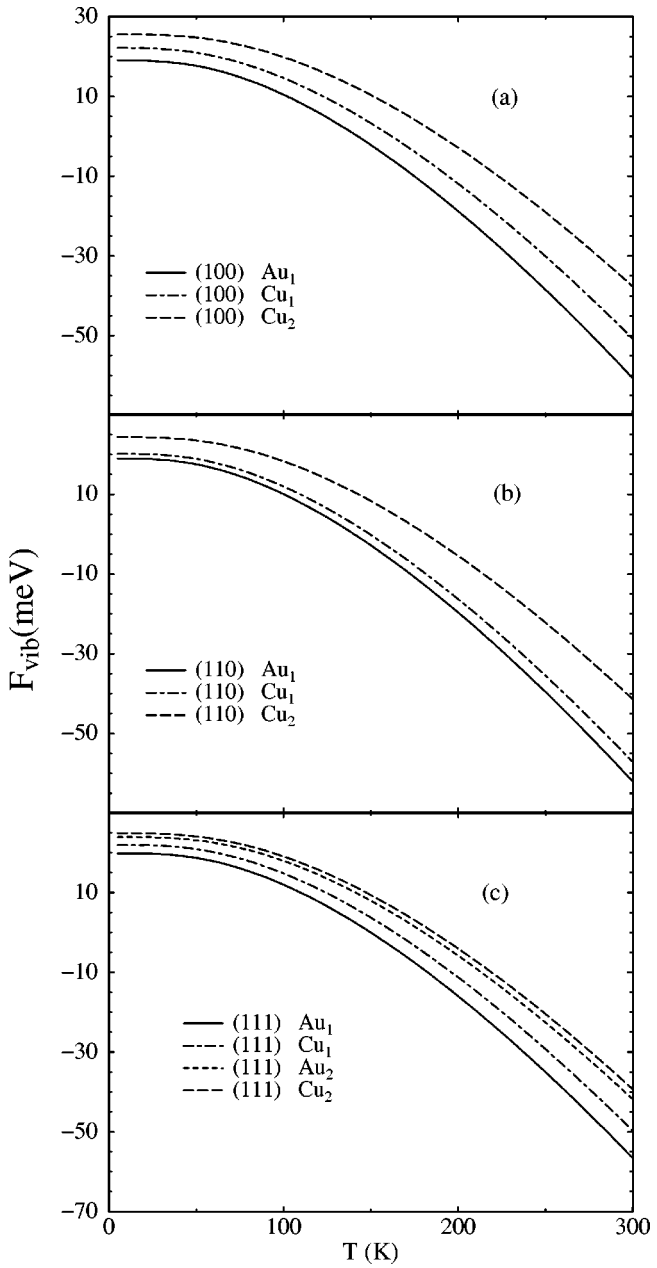

FIG. 11. Local vibrational free energy of Au and Cu atoms in the top two layers of Cu_3Au (a) (100), (b) (110), and (c) (111).

traceable to the characteristics of the LDOS's, as discussed earlier.

3. Local contributions to vibrational free energy

The temperature variation of the local vibrational free energies of the constituent atoms in the top two layers of the three surfaces follows directly from the discussion above of the local vibrational entropy. Nevertheless, as this is a key property, we present our findings in Fig. 11 and also tabulate the results for selected temperatures in Table VII. The similarities and differences in the relative contributions from the Au and Cu atoms are as expected from previous discussions. The vibrational contribution acts as a stabilizing factor for all these surfaces above 150 K (or so) by lowering the total free energy. Of course, at increasing temperatures anharmonic effects and changes in the potential energy surfaces are going to compete with any stabilizing feature seen here and surfaces will respond accordingly. The numbers presented in the table illustrate clearly that the vibrational contributions and their comparative differences on the three surfaces cannot be ignored in any consideration of surface disorder or dynamics.

4. Surface excess thermodynamic quantities

Finally, in Fig. 12, we display the calculated excess vibrational free energy, excess entropy, and the excess lattice heat capacity for Cu_3Au (100), (110), and (111) surfaces, for the temperature range 0–300 K. These curves illustrate unambiguously the net result of the discussion so far about the similarities and differences in the vibrational characteristics of the three surfaces: vibrational effects make the most striking contribution on $Cu_3Au(110)$. At 300 K, for example, the

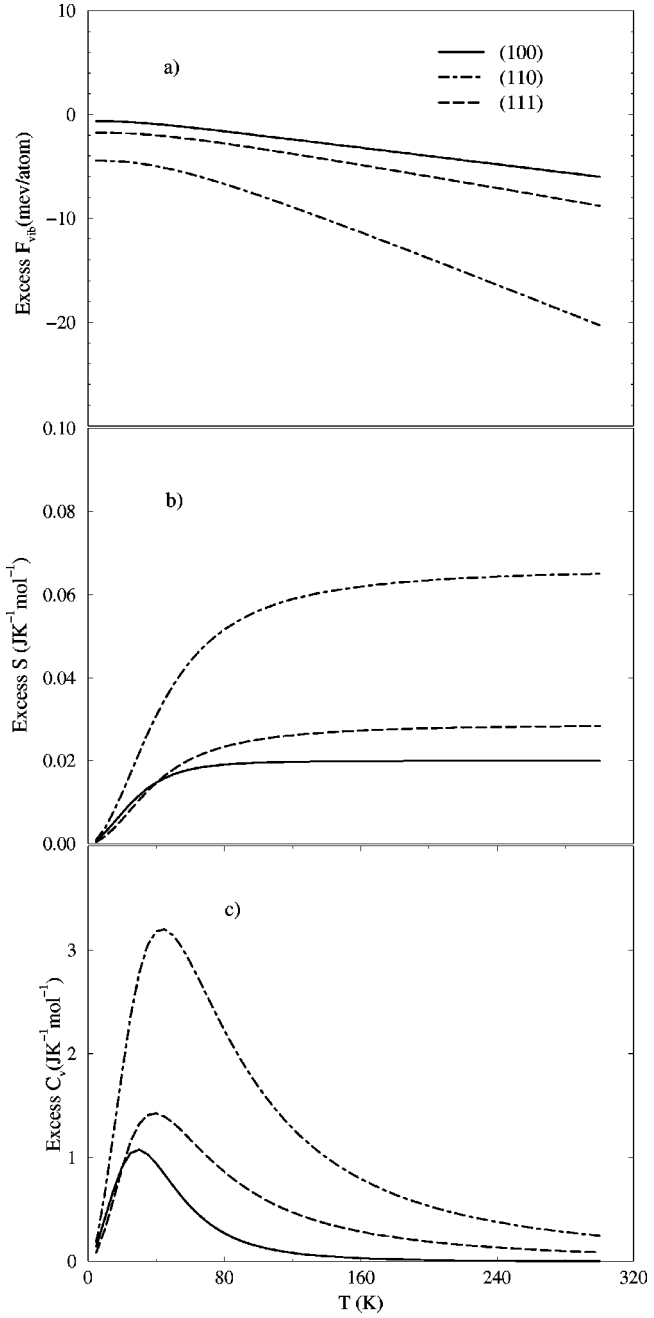

FIG. 12. A comparison of the excess surface thermodynamic functions (a) vibrational free energy (F_{vib}), (b) vibrational entropy (S_{vib}) and (c) lattice heat capacity (C_{vib}), for Cu_3Au (100), (110), and (111).

excess vibrational free energy causes a lowering of the total free energy of about 16 meV/atom, as compared to only a few meV/atom for the other two surfaces. Similarily, for the excess lattice heat capacity the most measurable deviation from the bulk value occurs for $Cu_3Au(110)$.

IV. SUMMARY AND CONCLUSION

In this comparative study of the structure, vibrational dynamics, and local and excess thermodynamic properties of the (100), (110), and (111) surfaces of Cu_3Au, we find surface effects to be most pronounced on (110), followed by (100) and (111). The most convincing measures of these differences are the local vibrational densities of states in Figs. 2–4, which show that, while for the (111) surface only the atoms in the top layer display deviation from bulklike behavior, for the (110) and (100) surfaces there are pronounced surface characteristics even for the atoms in the second layer. Interestingly, for the first and second layer atoms on $Cu_3Au(110)$ there is an overall enhancement of low frequency modes, while for $Cu_3Au(100)$ there is also the appearance of modes above the top of the bulk band. The surface related modes at both the low and high frequency ranges on $Cu_3Au(100)$ play a balancing role in the surface thermodynamic properties and lead eventually to lesser deviations of these characteristics from those of the bulk atoms, as compared to the effects on $Cu_3Au(110)$. On the latter surface the pronounced enhancement of the low frequency modes in the first and the second layer, and the near absence of modes in the higher frequency regime, cause a relatively larger decrease in the vibrational free energy with increasing temperatures. Thus vibrational free energy would tend to stabilize $Cu_3Au(110)$ preferentially over the other two surfaces. Since these surfaces are also prone to segregation and eventually to disordering, which may initiate much below the bulk disordering temperature, we would like to leave the discussion of the temperature dependent, relative stability of these surfaces for the future when we already have on hand the calculations of the dynamics and thermodynamics of disordered structures of these surface systems. The results presented here act as reference points with which the contribution of vibrational free energy to surface disorder may be evaluated. In the meantime, the local thermodynamic quantities calculated here, like mean square vibrational amplitudes of surface atoms and the local contribution to entropy and vibrational free energy, provide useful information to experimentalists and theorists working on these intriguing sets of bimetallic surface systems. We welcome, of course, any experimental data on the surface phonons or the surface vibrational density of states of these systems. It would be particularly exciting to determine whether modes exist above the bulk band on some, and not other, surfaces of Cu_3Au, using techniques like electron energy loss spectroscopy.

TABLE VII. Local vibrational free energy in meV/atom.

Atom	0 K	100 K	200 K	300 K
(100) Au_1	19	10	−19	−61
(100) Cu_1	22	15	−12	−51
(100) Cu_2	26	20	−3	−38
(110) Au_1	19	10	−20	−62
(110) Cu_1	20	12	−16	−57
(110) Cu_2	24	18	−6	−41
(111) Au_1	20	12	−16	−57
(111) Cu_1	22	15	−11	−50
(111) Au_2	24	18	−6	−42
(111) Cu_2	25	19	−4	−39

During the preparation of the manuscript we became aware of related work by Lekka *et al.*[27] on Cu_3Au surfaces. These authors use molecular dynamic simulations and a set of interaction potentials obtained within a tight-binding scheme to calculate the layer-by-layer structural and dynami-

cal properties of Cu_3Au (100), (110), and (111). There are some interesting differences in the results because of the usage of two types of interaction potentials. The general trends in the vibrational density of states are similar to those obtained by us, though not the comparative details. Perhaps this work will motivate these authors to calculate surface thermodynamic quantities and hence compare the dependence of the results on the nature of the interaction potential.

ACKNOWLEDGMENTS

We would like to thank S. Durukanoglu for discussions. This work was supported partially by the U.S. Department of Energy, Basic Energy Sciences Division, under Grant No. DE-FG03-97ER45650. Computations were carried out on HP SPP2200 funding partially by NSF under Grant No. CDA-9724289.

[1] C. T. Campbell, Annu. Rev. Phys. Chem. **41**, 775 (1990).
[2] U. Bardi, Rep. Prog. Phys. **57**, 939 (1994).
[3] J. M. Cowley, J. Appl. Phys. **21**, 24 (1950); Phys. Rev. B **77**, 669 (1950).
[4] H. Dosch, L. Mailander, H. Reichelt, J. Peisl, and R. L. Johnson, Phys. Rev. B **43**, 13 172 (1991).
[5] A. Stuck, J. Osterwalder, L. Schlapbach, and H. C. Poon, Surf. Sci. **251/252**, 670 (1991).
[6] F. M. Zhang, B. V. King, and D. J. O'Connor, Phys. Rev. Lett. **75**, 4646 (1995).
[7] S. Dietrich, in *Phase Transition and Critical Phenomena*, edited by C. Domb and J. Lebowitz (Academic, New York, 1988), Vol. 12.
[8] H. Reichert, P. J. Eng, H. Dosch, and I. K. Robinson, Phys. Rev. Lett. **74**, 2006 (1995); H. Reichert and H. Dosch, Science **354**, 27 (1996).
[9] L. Anthony, J. K. Okamoto, and B. Fultz, Phys. Rev. Lett. **70**, 1128 (1993).
[10] L. J. Nagel, L. Anthony, and B. Fultz, Philos. Mag. Lett. **72**, 421 (1995).
[11] P. D. Bogdanoff, B. Fultz, and S. Rosenkranz, Phys. Rev. B **60**, 3976 (1999).
[12] J. D. Althoff, D. Morgan, D. De Fontaine, M. Asta, S. M. Foiles, and D. D. Johnson, Phys. Rev. B **56**, 5705 (1997).
[13] R. Ravelo, J. Aguilar, M. Baskes, J. E. Angelo, B. Fultz, and B. L. Holian, Phys. Rev. B **57**, 862 (1998).
[14] V. Ozoliņš, C. Wolverton, and Alex Zunger, Phys. Rev. B **58**, 5897 (1998).
[15] T. M. Buck, G. H. Wheatley, and L. Marchut, Phys. Rev. Lett. **51**, 43 (1983).
[16] H. Niehus and C. Achete, Surf. Sci. **289**, 19 (1993).
[17] V. S. Sundaram, B. Farell, F. S. Alben, and W. D. Robertson, Phys. Rev. Lett. **31**, 1136 (1973).
[18] S. M. Foiles, Surf. Sci. **191**, 329 (1987); S. M. Foiles and M. S. Daw, J. Mater. Res. **2**, 5 (1987).
[19] M. S. Daw, S. M. Foiles, and M. I. Baskes, Mater. Sci. Rep. **9**, 251 (1993).
[20] W. E. Wallace and G. J. Ackland, Surf. Sci. Lett. **275**, L685 (1992).
[21] R. J. Kobistek, G. Bozzolo, J. Ferrante, and H. Schlosser, Surf. Sci. **307-309**, 390 (1994).
[22] L. Houssiau and P. Bertrand, Surf. Sci. **352-354**, 978 (1996).
[23] H. Niehus, Phys. Status Solidi B **192**, 357 (1995).
[24] S. W. Bonham and C. P. Flynn, Surf. Sci. **366**, L760 (1996).
[25] K. S. Dy, S. Y. Wu, and T. Spartlin, Phys. Rev. B **20**, 4237 (1979); S. Y. Wu, J. Cockse, and C. S. Jayanthi, *ibid.* **49**, 7957 (1994).
[26] B. Gans, P. A. Knipp, D. D. Kloeske, and S. J. Sibener, Surf. Sci. **264**, 81 (1992).
[27] Ch. E. Lekka, N. I. Papanicolaou, and G. A. Evangelakis (unpublished).